# Global vs. spatially resolved physical characteristics of extragalactic HII regions

ESTALLIDOS
de formación estelar

Jesús López-Hernández (INAOE-PhD)
Elena Terlevich (INAOE, Puebla, Mexico)
Roberto Terlevich (INAOE/IoA)
Fabio Bresolin (IfA, Hawaii)
Daniel Rosa-González (INAOE)
Ángeles Díaz (UAM, Madrid, Spain)
Rubén García Benito (IAA, Granada, Spain)
José Vílchez (IAA)
Guillermo Hägele (FCAG, La Plata, Argentina)

# Motivation

- Part of a programme to study the difference in the processes of star formation in the centre and disc environments (inner and outer: higher and lower Z regions) of nearby spiral galaxies.
- Chemical composition (and radial gradients) Aller (1942), Searle (1971), Smith (1975). Abundance gradients and galactic chemical evolution.
- Search for possible physical parameters variation inside each starforming region.

- Three HII regions in M33 were observed with PMAS (PPak mode)@3.5m telescope in CAHA (Spain). Two central positions and IC 132, ~19’ (4.69kpc) NW of the centre of the galaxy. (López Hernández et al. MNRAS 2013)
- Three giant HII regions in M101 were observed with GMOS@Gemini-N: NGC 5461, Searle 5 and Hodge 1013. (López Hernández PhD, INAOE, 2013)
- Due to the respective distances and instrumentation, both sets of observations correspond to a similar physical resolution in both galaxies.

# M33 properties

| | |
|---|---|
| Designations | Messier 033, Triangulum Galaxy, NGC 0598,UGC 01117, PGC 005818 |
| Classification | SA(s)cd HII |
| Major Diameter | 70.8 Arcmin |
| Minor diameter | 41.7 arcmin |
| Position Angle | 23 deg |
| Distance | 840 kpc (Freedman et al. 2001) |
| Redshift | -0.000597 ± 0.000010 |
| Inclination angle | 53.52 deg (Corbelli & Salucci 2000) |
| PPak scale | 3.23 pc/arcsec (8.65 pc/fibre ) |

Source is NED unless otherwise specified.

- [OIII] 4363Å shifted to 4360.1 too close to HgI 4358.3 in CAHA sky.
- 12 + logO/H between 8.9 (center) and 8.5 (IC 132)

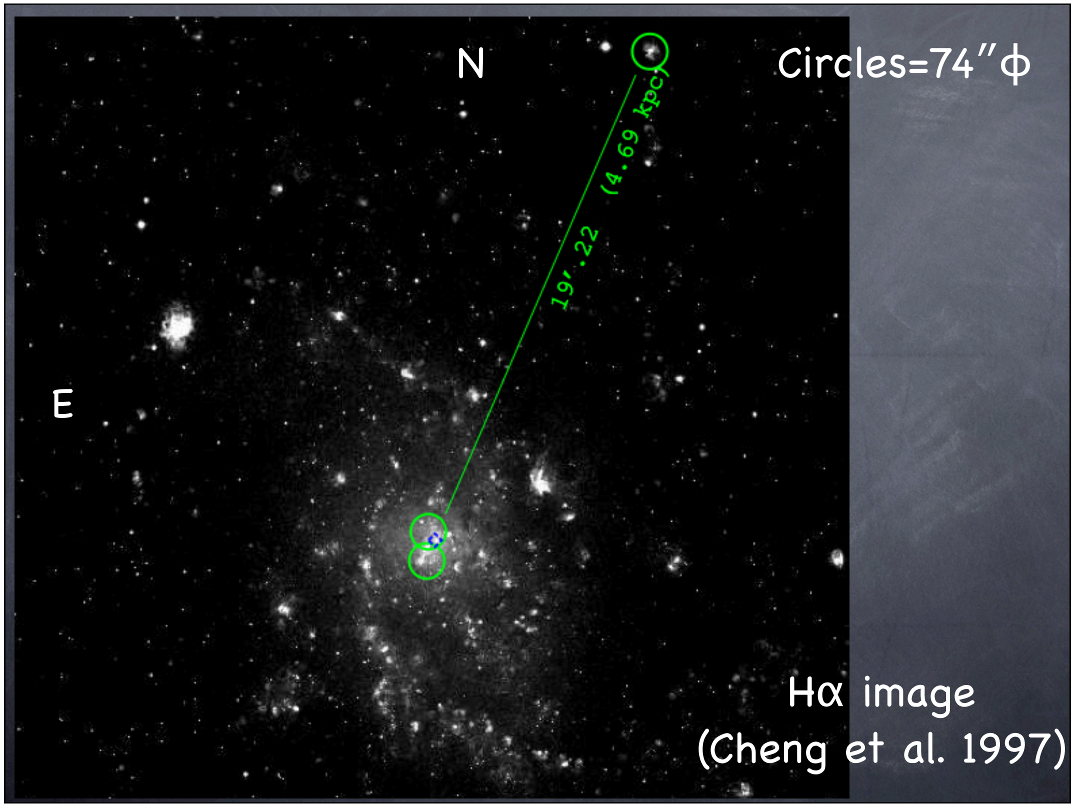
N
Circles=74″ϕ
19′.22 (4.69 kpc)
E
Hα image
(Cheng et al. 1997)

# Calar Alto Data

- PMAS@3.5m in CAHA Fiber Package PPak Mode.
- 331 science fibers FOV 74″×64″ and 6 bundles (6 fibers each) @72″ from the centre for the sky.
- Projected fiber diameter: 2″.68 (10.9pc).
- Filling factor of the science packet 60%.
- Wavelength coverage 3591 - 6996 (3.4 Å/pix); 6873-10186 (3.4 Å/pix); 6100-6650 (0.64 Å/pix). 2×2binning. Average seeing 1″.
- 3 dithered pointings for each object.
- (Thanks to Sebastián Sánchez et al. E3D reduction packages)

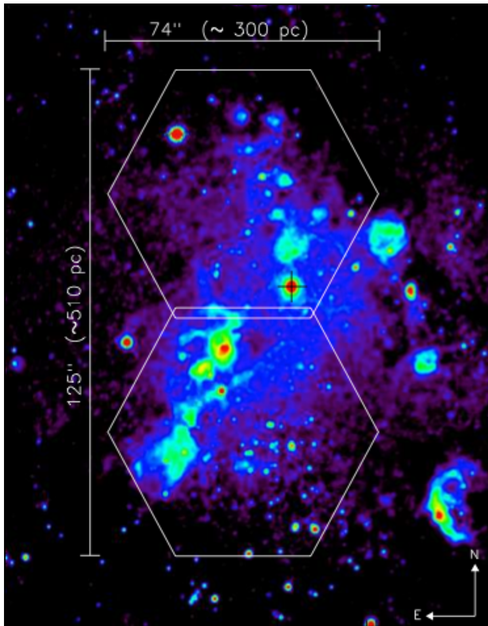


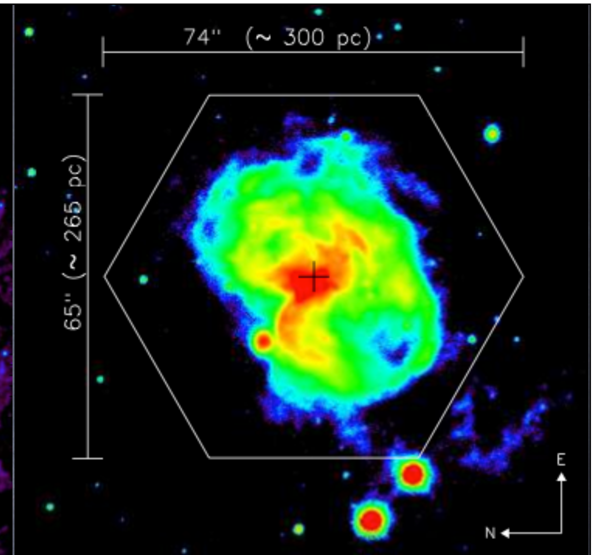


IC 132

Central fields, 3″ overlapped

M33 X-8 (ULX)

Adopted distance: 840kpc

Hα, NOAO Science Archive (Massey et al. 2006)

# M101 properties

Table 3.1: M101 characteristics

| | |
|---|---|
| Other names | NGC 5457, Pinwheel galaxy |
| R.A (2000J) | $14^h03^m12.5^s$ |
| DEC. (2000J) | $+54°20''56''$ |
| Redshift | $0.000804 \pm 0.000007$ |
| Distance[a] | $6.70 \pm 0.34$ [Mpc] |
| Inclination[b] | $18° \pm 3$ |
| Position angle[b] | $39° \pm 2$ |
| Disk isophotal diameter[c] | $14'.42$ |
| Systemic velocity[b] | $242.5 \pm 5$ [km $s^{-1}$] |
| Abundance range[d] | $(8.74 \pm 0.17)$ — $(7.55 \pm 0.07)$ |

References: [a]Freedman et al. (2001) [b]Bosma et al. (1981) [c]de Vaucouleurs et al. (1991). [d]Li et al. (2013) In 12+log(O/H) scale. Values are for the inermost region (H493, $R/R_o$=0.1) and the most external (SDH323, $R/R_o$=1.2). Other values were obtained from NED.

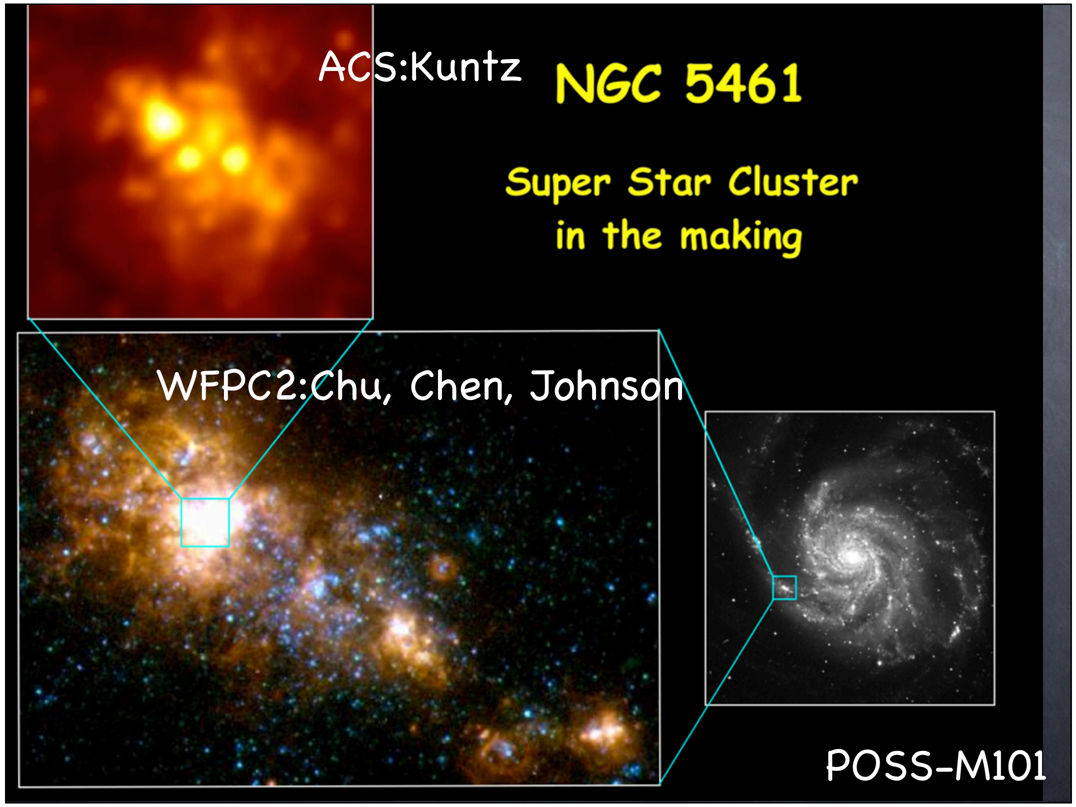
ACS:Kuntz
NGC 5461
Super Star Cluster
in the making
WFPC2:Chu, Chen, Johnson
POSS-M101

# M101 (STScI Digitized Sky Survey POSS B)

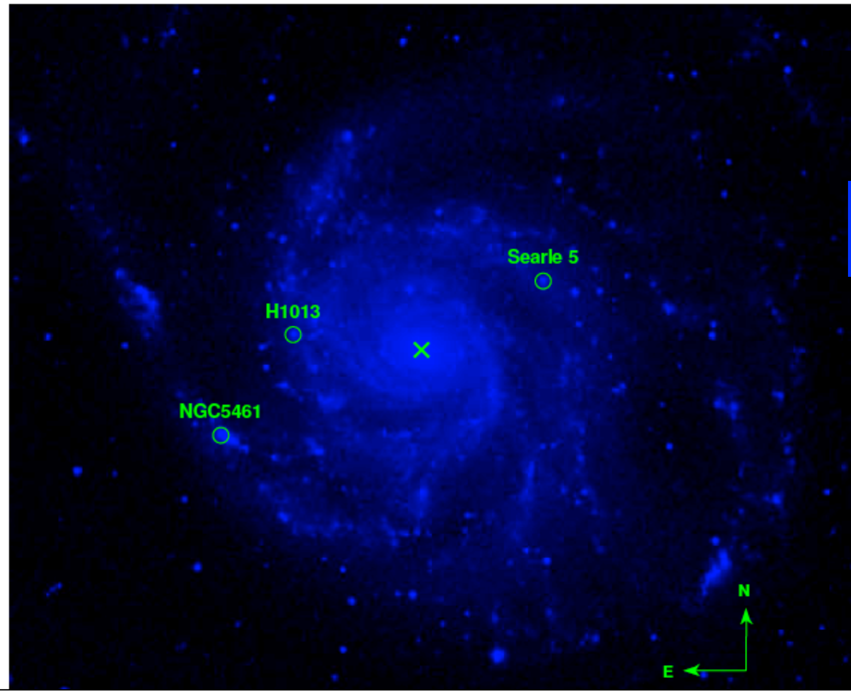


○=10″
~ 320 pc

# GMOS Data

- GMOS@8m in GEMINI-N.
- Array of hexagonal lenslets; each one coupled to a fiber; detector: 3 2048x4608 EEV chips arranged in a row. 500 fibers for the object and 250 for the sky @1′ away from the object. Spatial sampling 0″.2/fiber.
- Pixel size 13.5μm; plate scale 0″.0727/pix.
- 1-slit mode: FOV 5″×3.5″(science); 5″×1.75″ for sky.
- Wavelength coverage 3650 - 6400 (0.46 Å/pix); 6350-9150 (0.47 Å/pix) 2×2binning. Average seeing 0.5″. Photometric conditions.
- (Thanks to Gelys Trancho et al. GMOS reduction packages)

# M101 Journal of observations (Gemini-N Jan/2007)

| Object | RA (J2000.0) | DEC (J2000.0) | Exposure [s] 3650 - 6400 Å | Exposure [s] 6350 - 9150 Å |
|---|---|---|---|---|
| NGC 5461 | $14^h03^m40.5^s$ | $54°19'01''$ | 3×1800 | 3×1800 |
| Searle 5 (S5) | $14^h02^m54.6^s$ | $54°22'27''$ | 3×1800 | 3×1800 |
| Hodge 1013 (H1013) | $14^h03^m30.7^s$ | $54°21'14''$ | 3×1800 | 2×1800 |

Average seeing was 0.″5

| Object | R(′) | D(″) |
|---|---|---|
| NGC 5461, S7, H1105 | 0.34 (9.4kpc) | 30 |
| S5, H336 | 0.22 (6.0kpc) | 11 |
| H1013, S3 | 0.19 (5.4kpc) | 14 |

R=deprojected galactocentric distance

D=Size

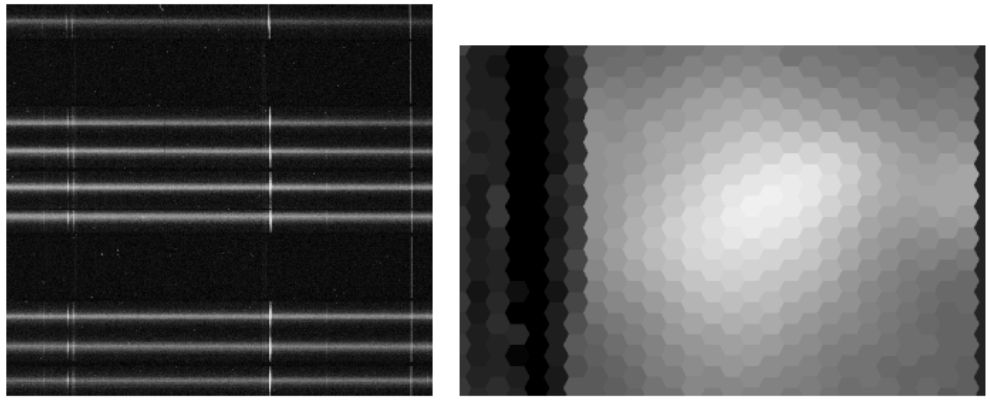

Figure 3.2: Left: Section of the Row Stacked Spectra (RSS) for NGC 5461. Right: Section of the reconstructed white-light image with the hexagonal lenslets structure of the instrument. The left side are fibers dedicated to the sky. Each lenslet has a projected diameter of 2″.

Jesús López PhD 2013, INAOE

# Sky subtraction difficulties (M33)

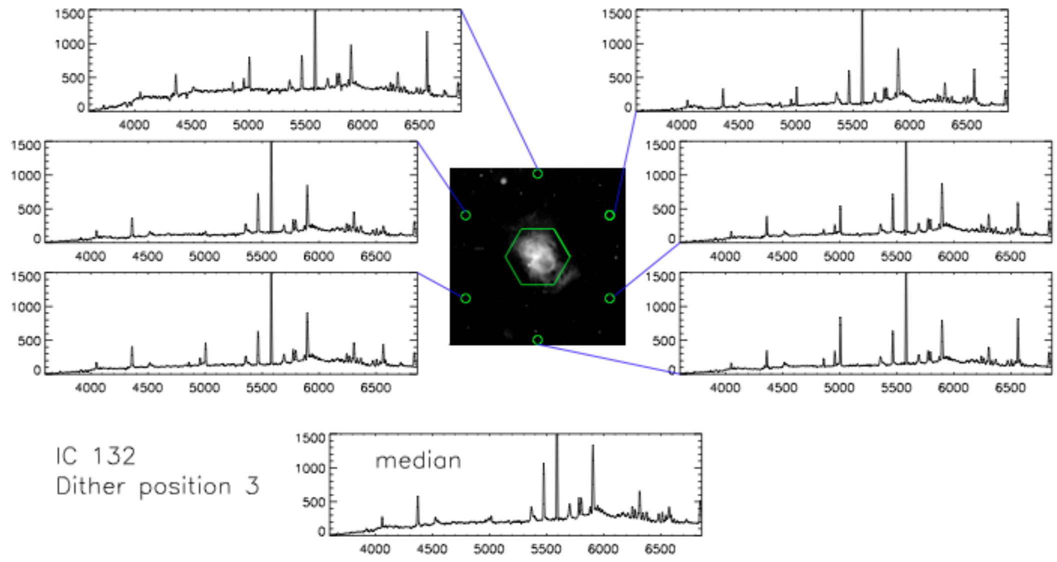

# Atmospheric absorption (M33)

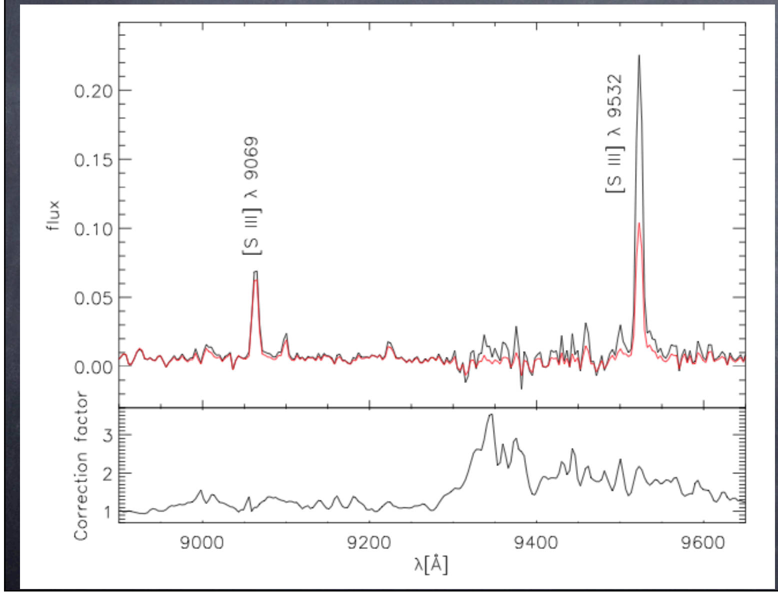


— Uncorrected

— Corrected

# Differential Armospheric Refraction
# S5-M101

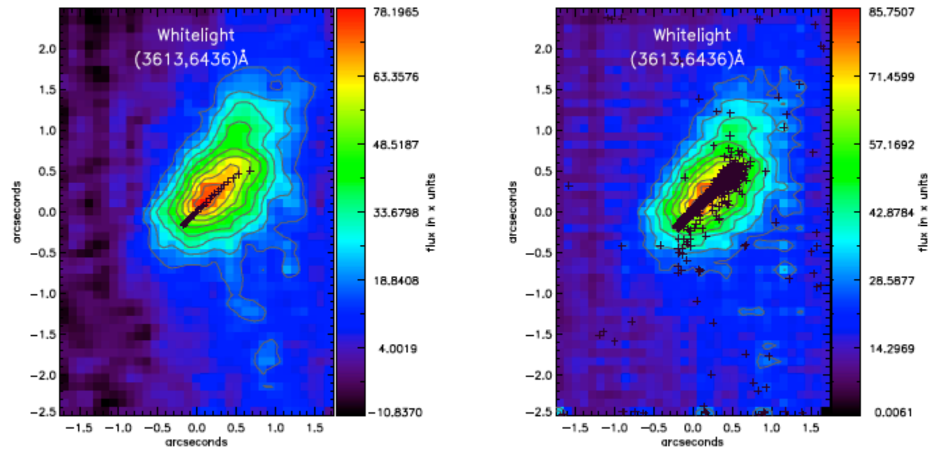


Figure 3.4: Left: Displacement due to DAR measured with different widths. Left: Displacement measured using 200 Å bands. Right: measured for each wavelength. In each panel the bluest wavelength is to the right and the reddest to the left. The background images are whitelight for Searle 5

# IC 132 Global spectrum

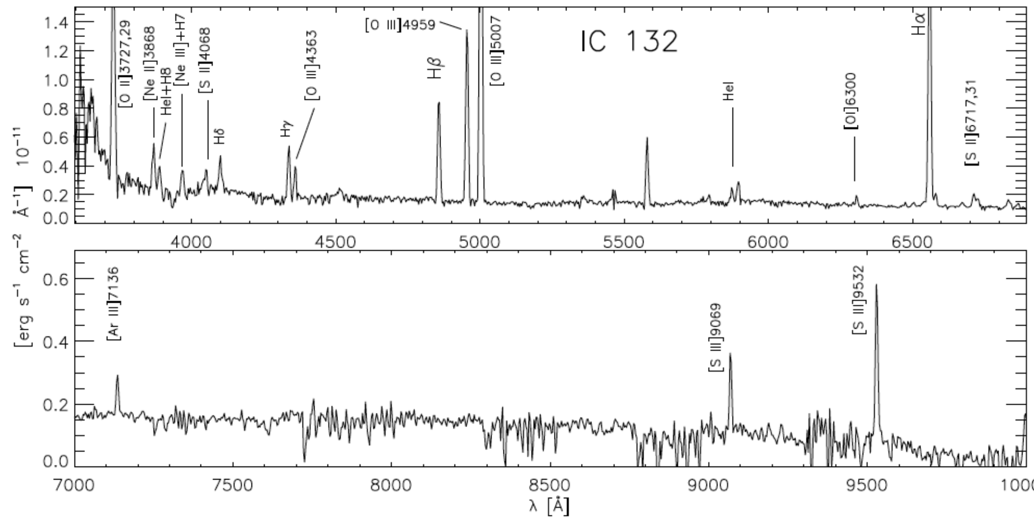

# NGC 5461 Global spectrum

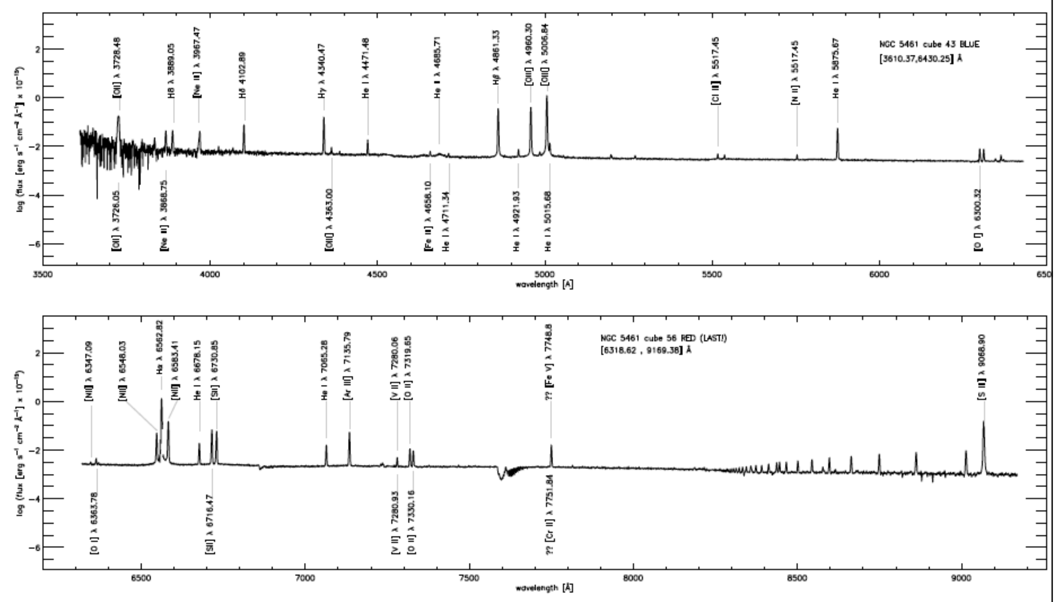

# Determining the gas physical conditions

Some ions forbidden emission lines can be used to determine $T_e$. For example, those corresponding to levels $2p^2$ of ions: $O^{2+}$, $N^+$, $S^{2+}$

[OIII]
λλ4959, 5007Å

[OIII]
λ 4363 Å

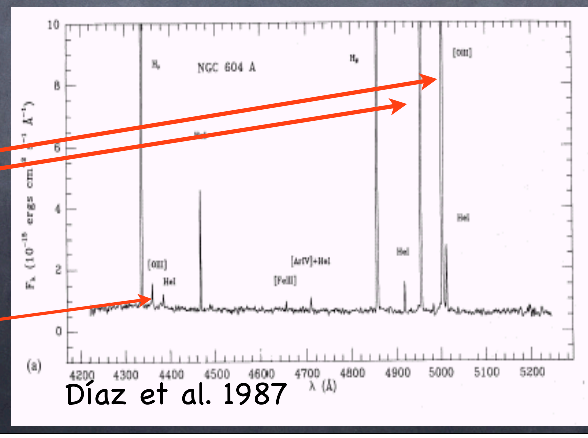

Díaz et al. 1987

Region A
in NGC 604

Temperature from collisional transitions between similar energy levels.

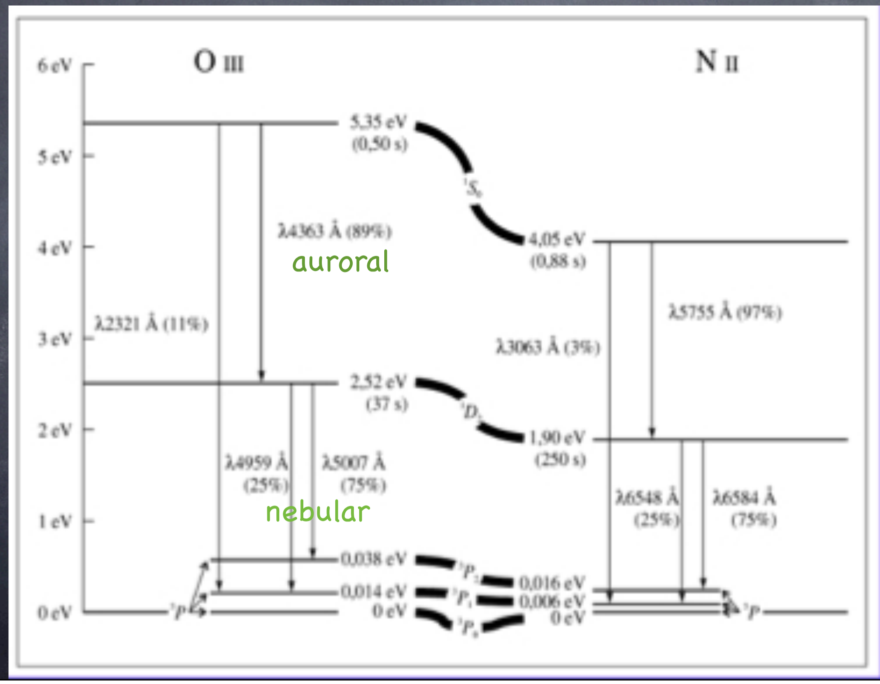

For the [OIII] lines:

$$\frac{j_{\lambda 4959} + j_{\lambda 5007}}{j_{\lambda 4363}} = \frac{7.73 \exp\left[\,(3.29 \times 10^4)/T\,\right]}{1 + 4.5 \times 10^{-4}\,(N_e/T^{1/2})}.$$

TEMPERATURE

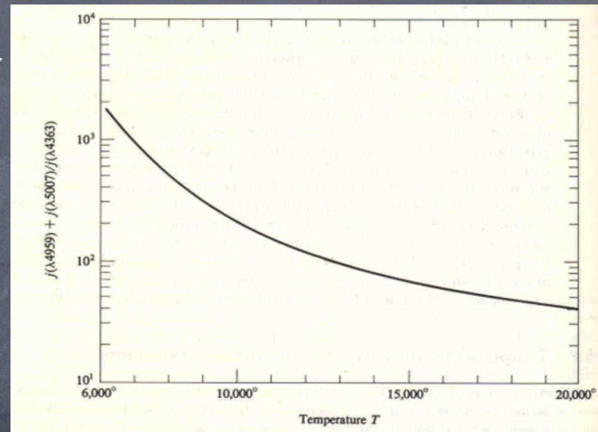


FIGURE 5.1
[O III] ($\lambda$4959 + $\lambda$5007)/$\lambda$4363 intensity ratio (in low-density limit $N_e \to 0$) as a function of temperature. Accurately calculated values shown here are indistinguishable from approximation of equation (5.4) using mean values of $\Omega$.

For the [NII] lines:

$$\frac{j_{\lambda 6548} + j_{\lambda 6583}}{j_{\lambda 5755}} = \frac{6.91 \exp\left[(2.50 \times 10^4)/T\right]}{1 + 2.5 \times 10^{-3}\,(N_e/T^{1/2})}.$$

Electron density can also be determined from ratios of certain emission lines.
e.g. [OII] y [SII]

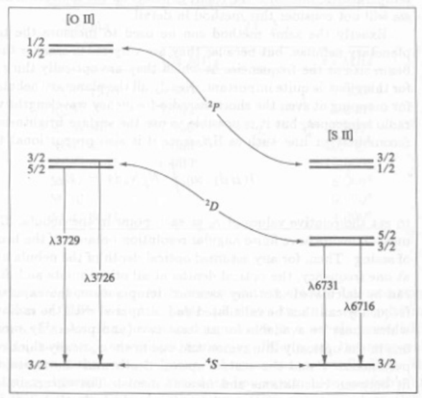


FIGURE 5.2
**Energy-level diagrams of the $2p^3$ ground configuration of [O II] and $3p^3$ ground configuration of [S II].**

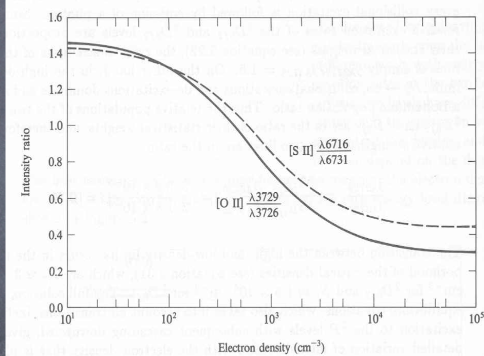


FIGURE 5.3
Calculated variation of [O II] (*solid line*) and [S II] (*dashed line*) intensity ratios as function of $N_e$ at $T = 10,000°$ K. At other temperatures the plotted curves are very nearly correct if the horizontal scale is taken to be $N_e(10^4/T)^{1/2}$.

DENSITY

Once temperature and density have been determined, ionic abundances can be derived from the intensities of the corresponding emission lines.

DIRECT CHEMICAL ABUNDANCES

$$\frac{X^{+i}}{H^{+}} = \frac{I(\lambda, X^{+i})}{I(H_{\beta})} \frac{\epsilon(H_{\beta})}{\epsilon(\lambda, x^{+i})}$$

- When $T_e$ and $N_e$ are not possible --> empirical calibrations.

# Empirical Calibration of the parameter $R_{23} = O_{23}$

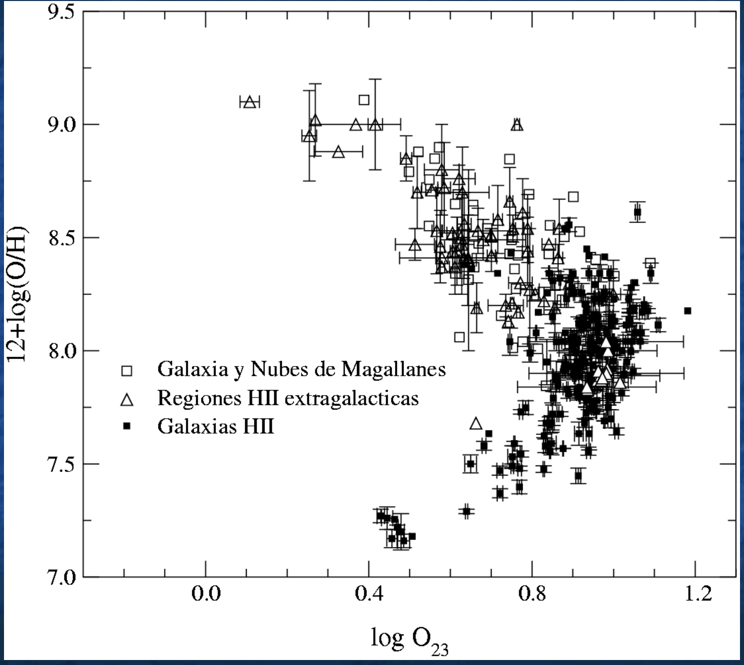

**Empirical calibrations rest on direct $T_e$ measurements in the low metallicity regime (high excitation) while requiring the use of theoretical models in the high metallicity (low excitation) regime.**

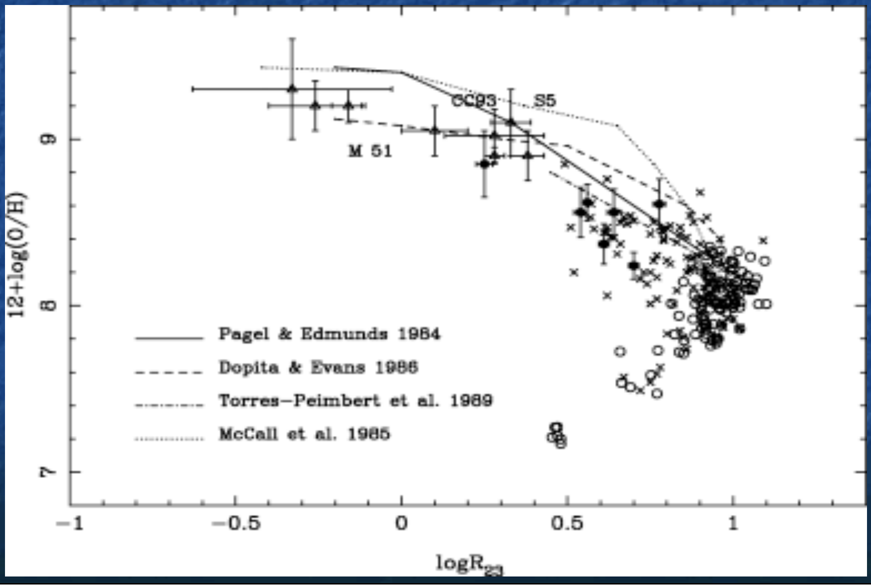

## ALTERNATIVE PARAMETER $S_{23}$

$$S_{23} = ([SII]+[SIII]) / H\beta$$

Also produced in massive stars. S/O constant.
Spectroscopically, lines are analogous to the oxygen ones but, because of their longer wavelength, their contribution to cooling should be more important at low temperatures.
Besides, they are less sensitive to $T_e$ , so the inversion of the relation should occur at higher metallicities.

The relation will remain univalued up to higher metallicity values.

# Calibration of the abundance parameter $S_{23}$

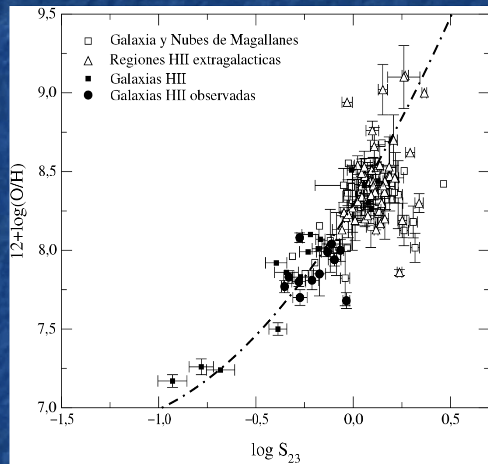


*Díaz & Pérez-Montero 2000*

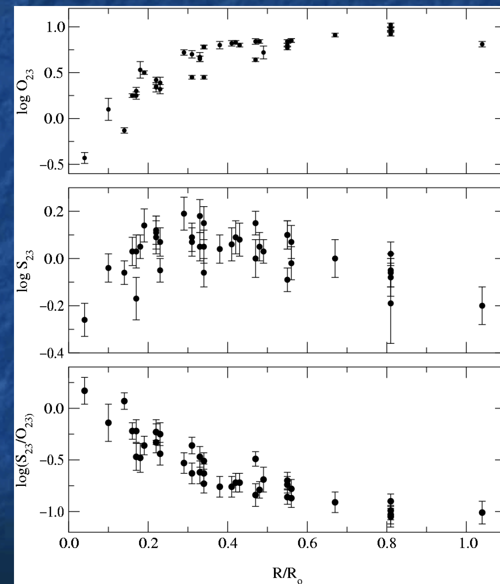

# Other abundance calibrators

N2 = I(6584 Å)/I(Hα) (Denicoló et al., 2001).

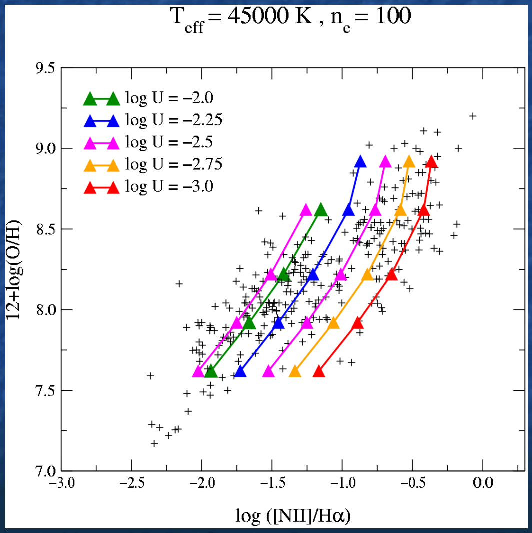


- No uncertainties due to reddening or to flux calibration and is univalued with metallicity over the whole range.
- But it shows scattering due to anticorrelation with the degree of ionisation and to the uncertainty on the N/O value.

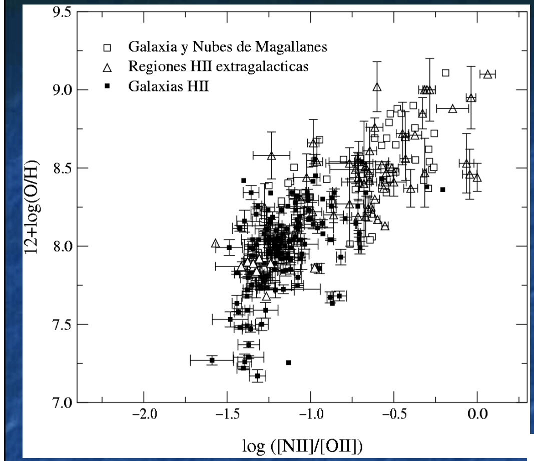


• [NII]/[OII] and [NII]/[SII] could indicate metallicity for values of 12+log(O/H) ≥ 8.6 (Kewley & Dopita, 2002).

•But observational scatter is similar that of N2, with the added problem that is not valid at low metallicities.

The parameter log [OIII]/[NII] , originally proposed by Alloin et al in 1979 has been revived by Pettini & Pagel (2004) to be used for intermediate redshift objects.

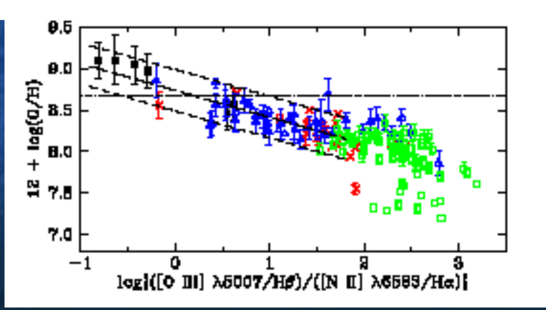

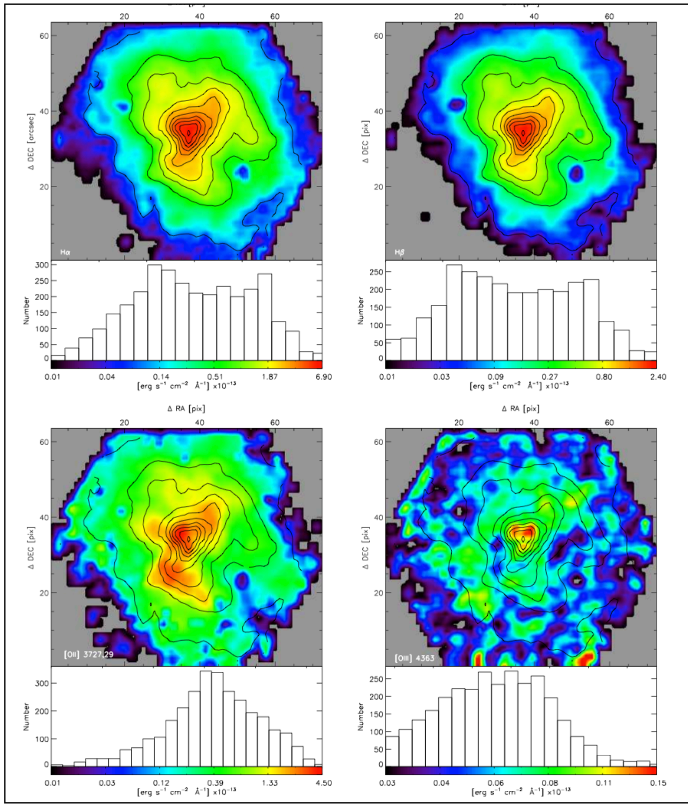


IC 132

Hα Hβ

[OII] [OIII]
3727 4363

S/N>5

except auroral
[OIII] and [SIII]
S/N>2

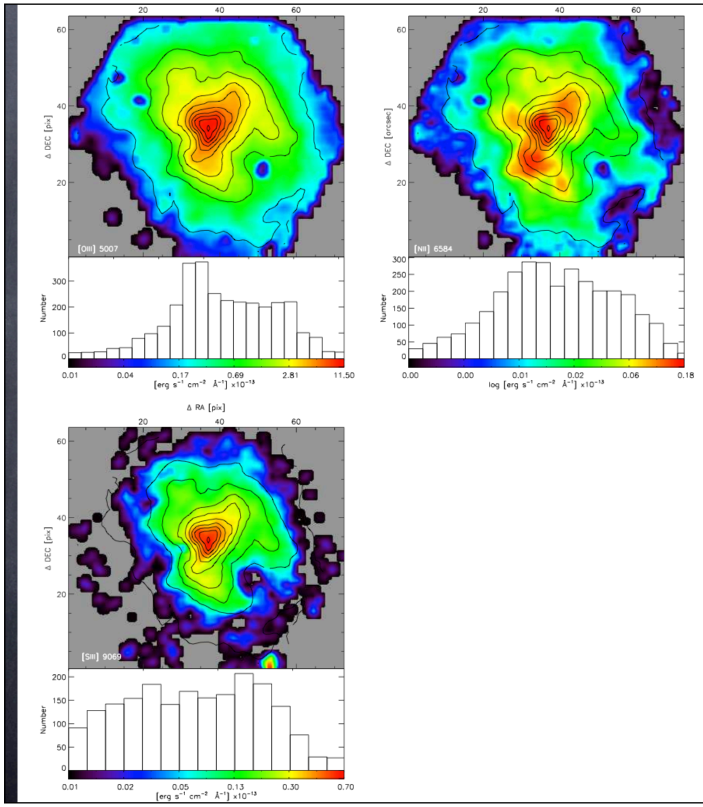


# IC 132

[OIII] 5007

[NII] 6584

[SIII] 9069

# HR data

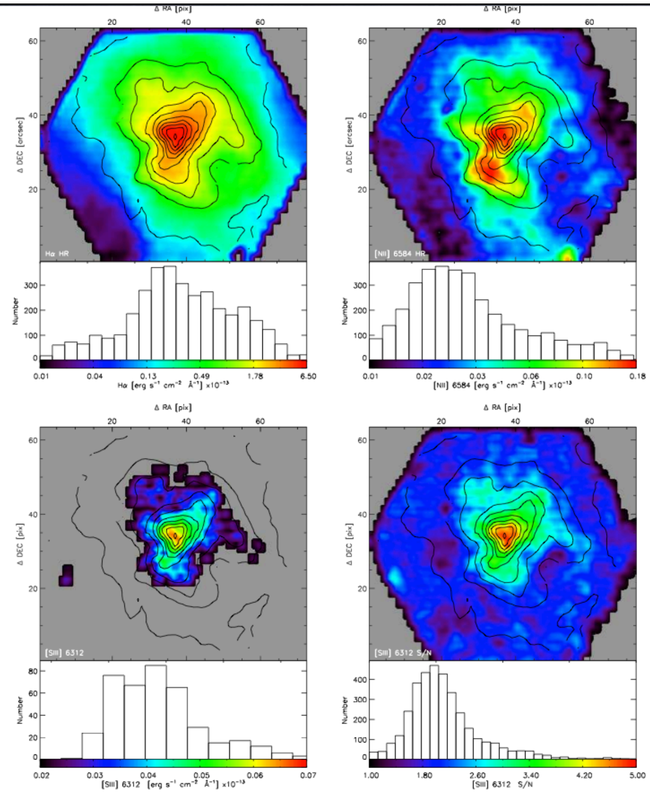

Hα

[NII] 6584

[SIII] 6312

[SIII] S/N

We used to take for granted homogeneity inside a region (e.g. Vílchez et al. 1988)

Line ratios variation along regions of NGC604-M33 (long slit spectra)

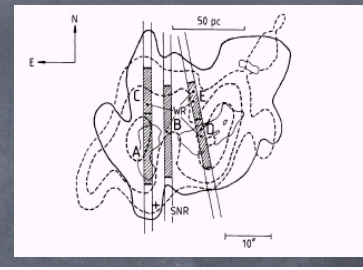


*A.Díaz et al. 1987, MNRAS, 226, 19*

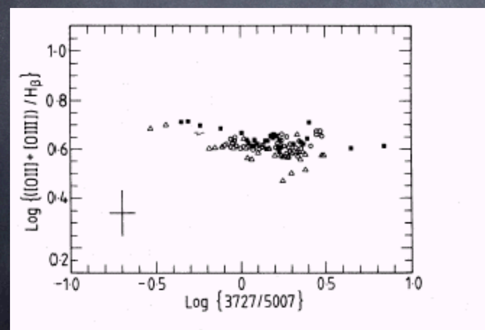


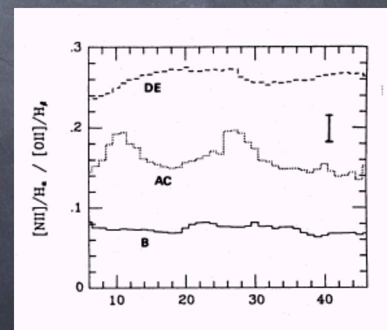

# C(Hβ)- M101

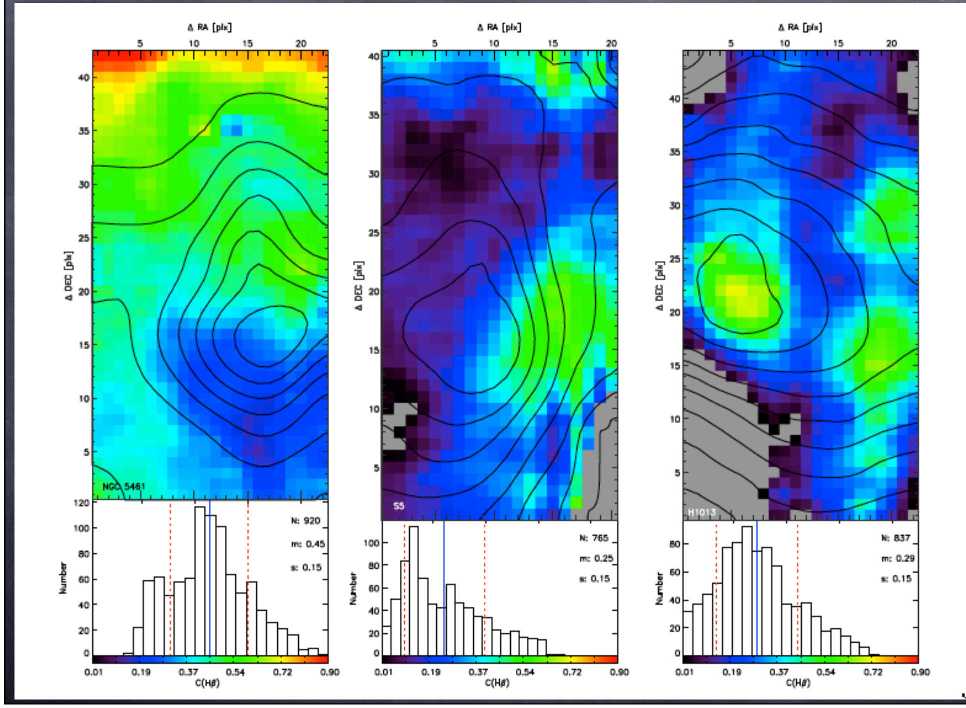

Δ RA [pix]
Δ DEC [pix]
NGC 5461
N: 920
m: 0.45
s: 0.15
S5
N: 765
m: 0.25
s: 0.15
H1013
N: 837
m: 0.29
s: 0.15
Number
C(Hβ)

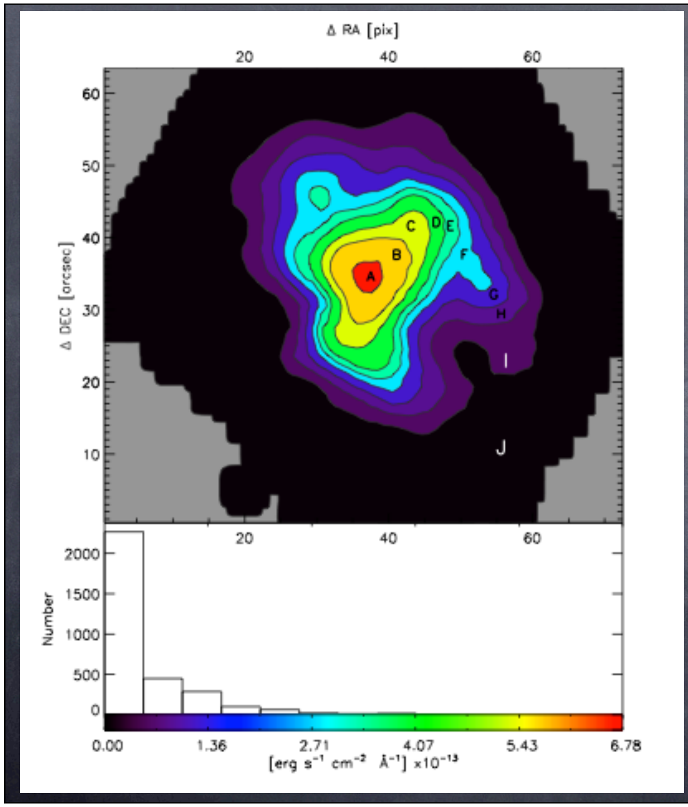


# Apertures defined on Hα isocontours (IC 132)

# Empirical metallicity estimators R23, N2, O3N2

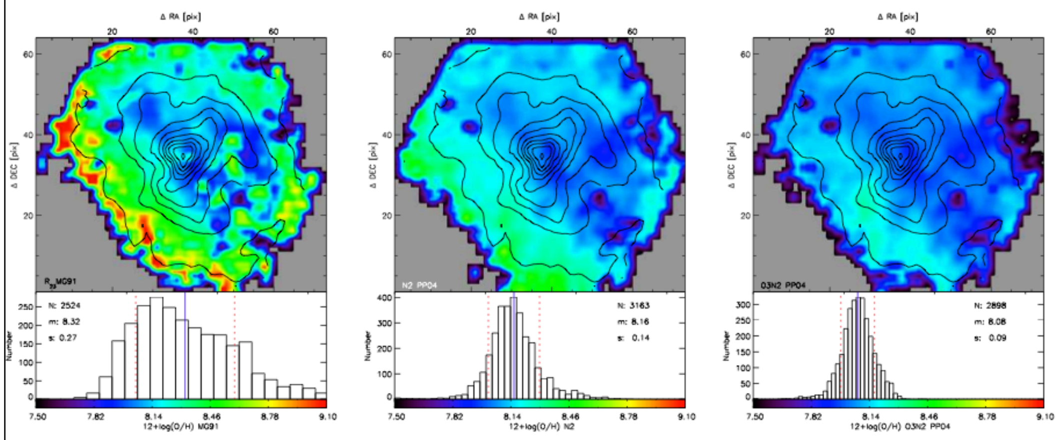

# [NII]/[OII] to separate upper and lower branch of R23;

vertical dashed line from Kewley and Ellison (2008)

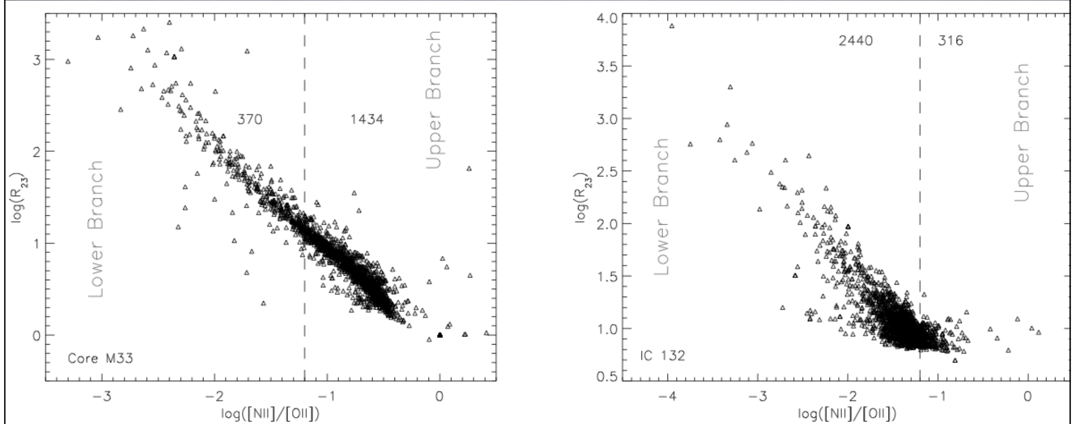

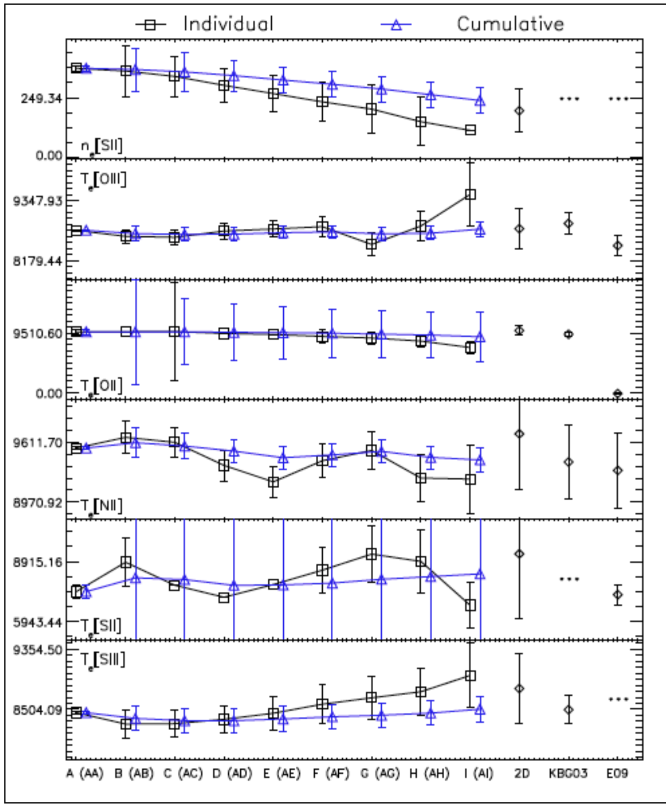


NGC5461 in M101 line $T_e$

2D=mean of distribution

KBG03=Kennicutt+ 03

E09=Esteban+ 09

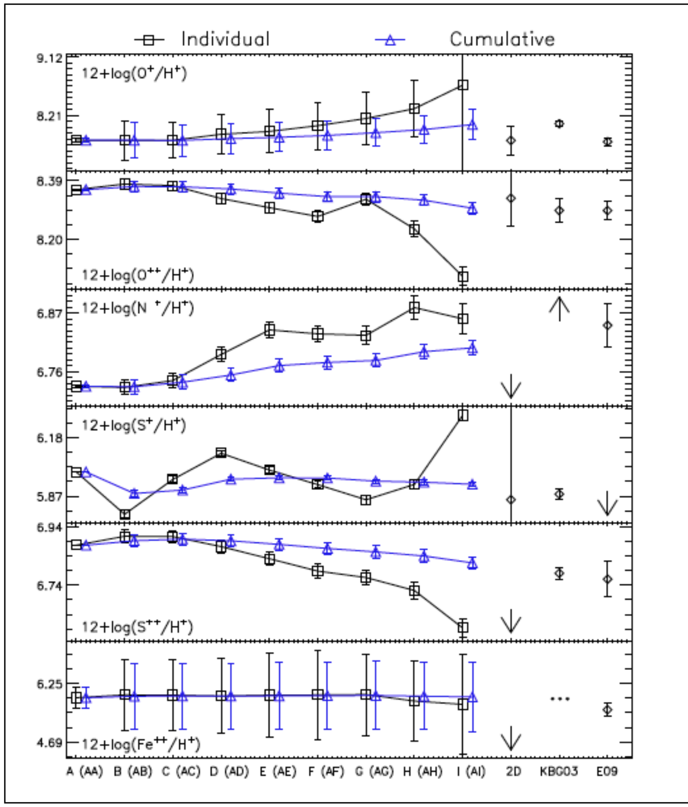


Ionic abundances NGC5461 in M101

# NGC5461

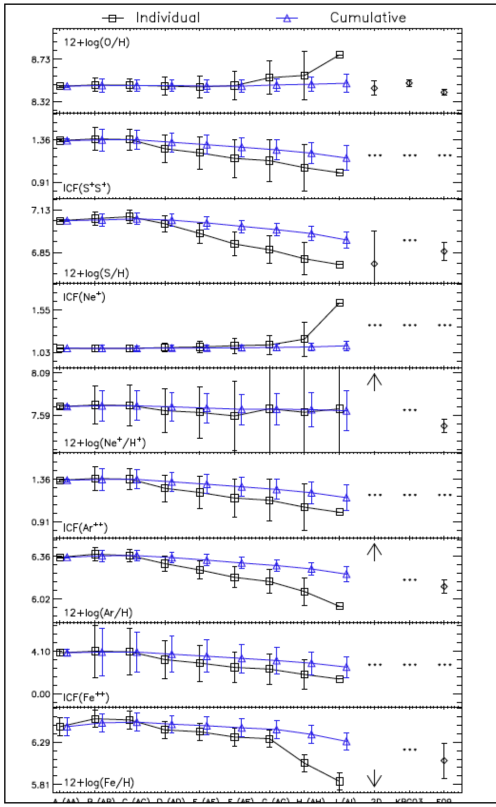


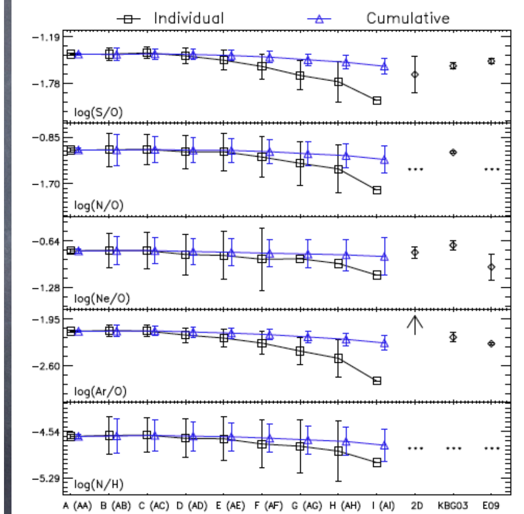


Figure 3.28: Same as 3.25 for abundance ratios.

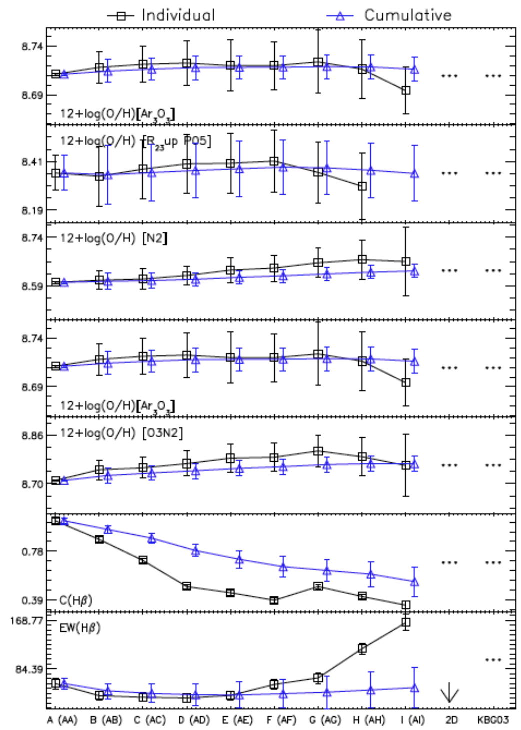


Figure 3.30: Radial trends for S5 empirical method abundances.

S5 in M101, empirical abundances

# Sobering thought

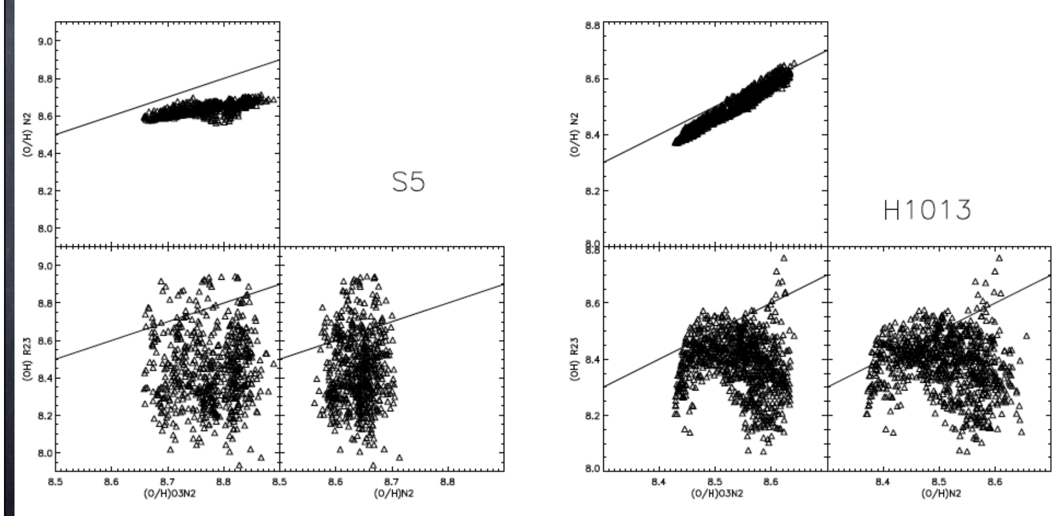

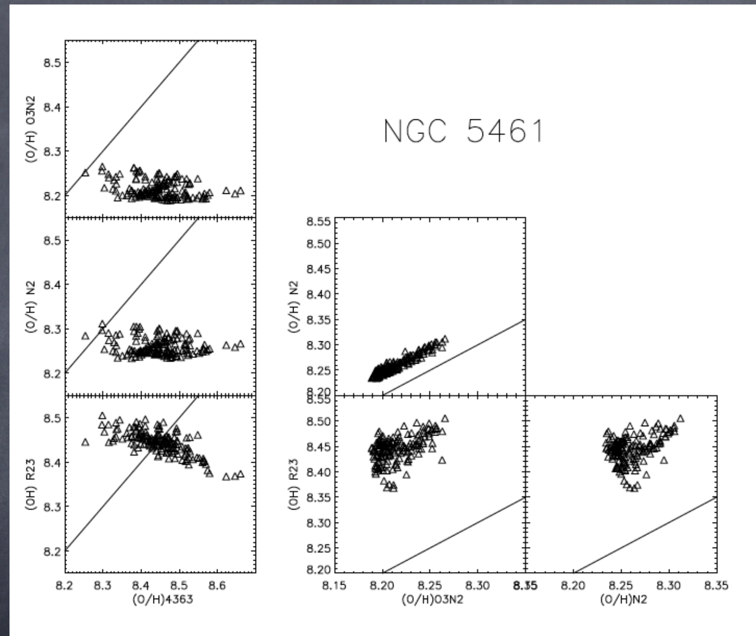
NGC 5461
(O/H) O3N2
(O/H) N2
(OH) R23
(O/H)4363
(O/H)O3N2
(O/H)N2

# Diagnostic diagrammes:

## [OIII]5007/Hβ, [NII]6584/Hα, [SII]6717,31/Hα

IC 132

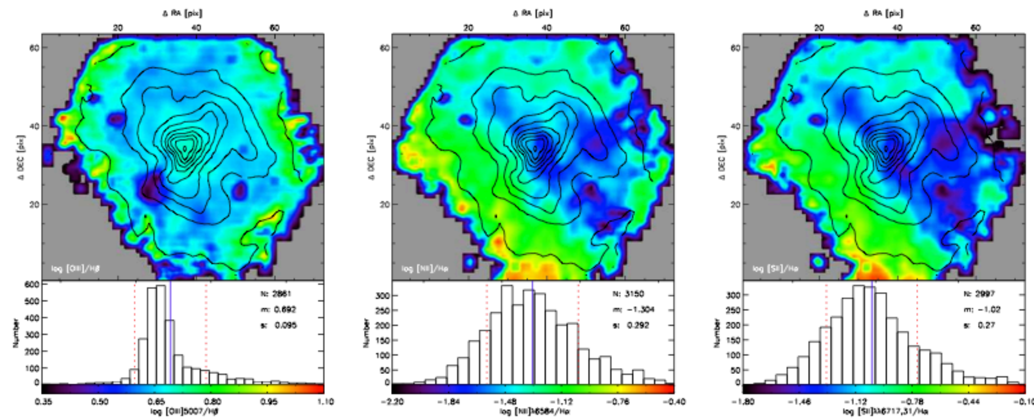

# BPT diagrammes (M33);

boundaries: Kewley+Dopita2002 (solid), Kauffmann+2003 (dotted), Stasińska+2006 (dashed)

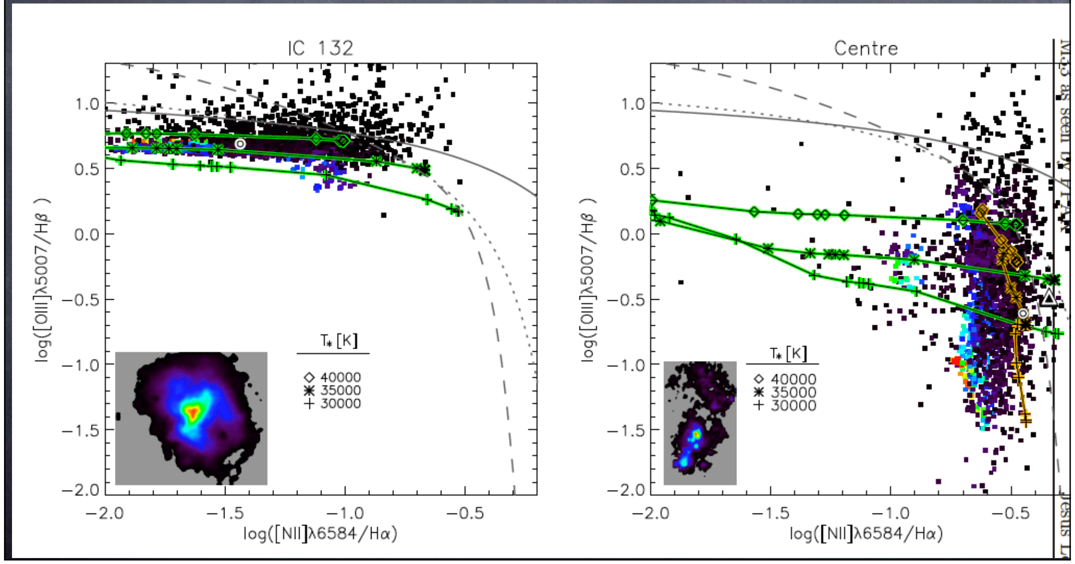

# BPT diagrammes for M101

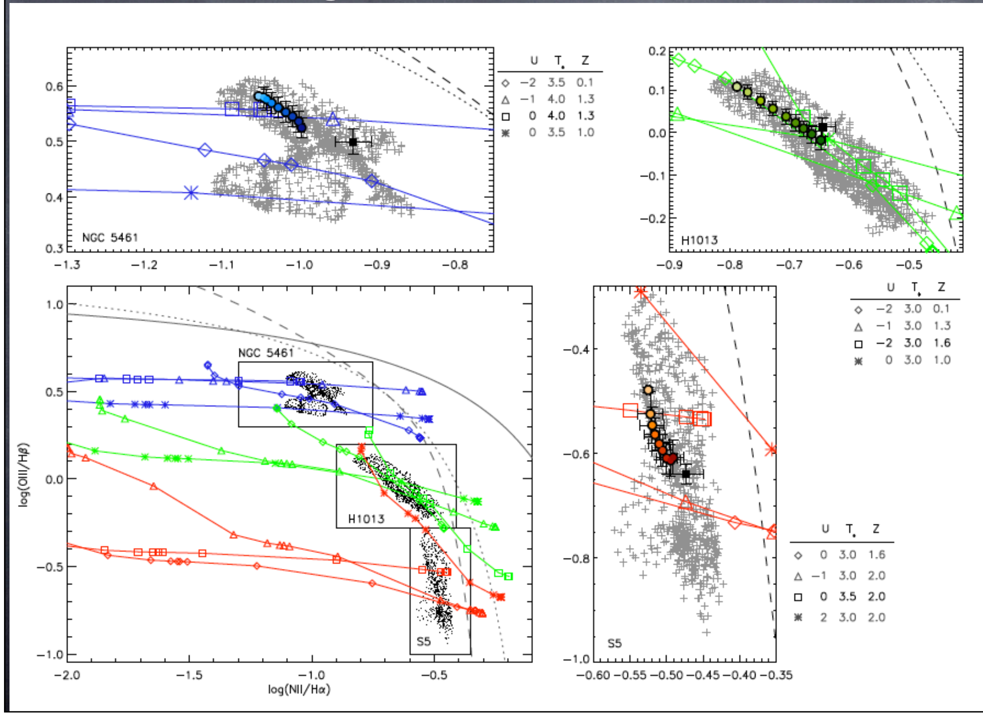

# Synthetic observations of pillar-like structures in optical emission lines.

(B. Ercolano et al. 2012, MNRAS)

$_{I}$VINE (Gritschneder) and MOCASSIN (Ercolano+)

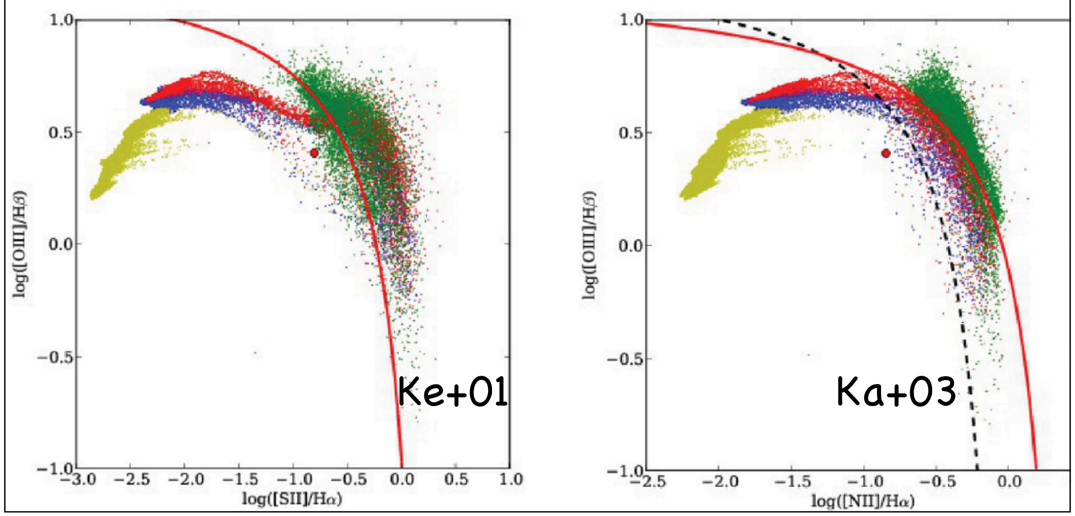

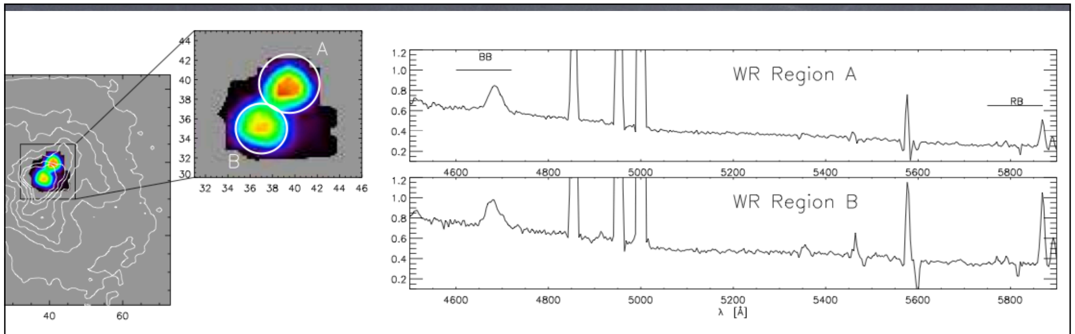


## IC 132 in M33

- Values are consistent with the presence of 21 WN7 in A and 24 WN7 Wolf-Rayet stars in B

| region | log(L) erg $s^{-1}$ | EW(BB) Å | BB/H$\beta$ |
|---|---|---|---|
| A | 37.84 | 15 | 0.38 |
| B | 37.89 | 13 | 0.41 |

# M101 regions

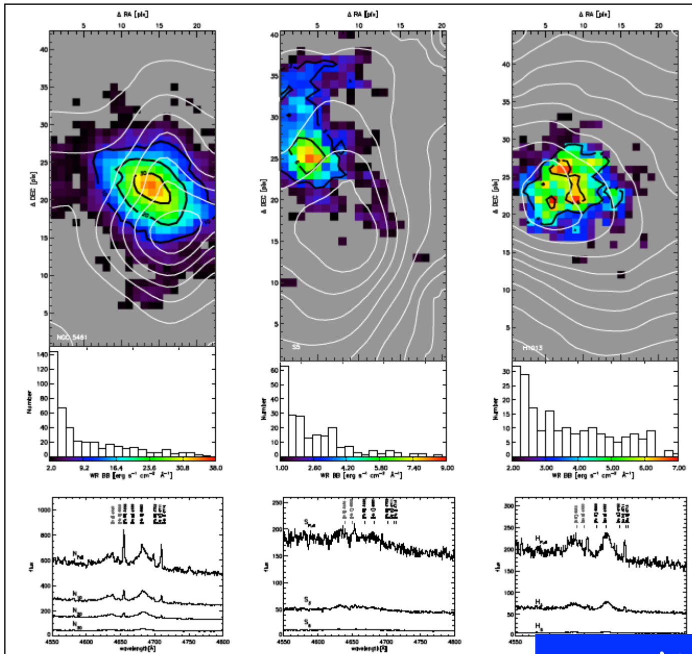

Figure 3.41: Maps for the blue bump (BB). The integration
4700 Å without narrow lines contribution. Black contours
with levels indicated. White contours are from the Hα ma
panels show the BB spectral range for each aperture as in
upper panel maps.

WR Blue Bump
4600Å - 4700Å
nebular lines subtracted

# Number of WN7 estimated from the BB

Table 3.18: Wolf Rayet BB, luminosity, EW and the estimation of the number of WN7 stars.

| | Zone | BB[a] | log L(BB) | EW(BB) | N(WN7) |
|---|---|---|---|---|---|
| | $N_{Full}$ | 4.82±0.24 | 38.41±0.03 | 8.92±0.40 | 83 |
| NGC 5461 | $N_{10}$ | 8.94±0.32 | 38.15±0.02 | 9.76±0.34 | 45 |
| | $N_{20}$ | 11.56±0.39 | 37.89±0.02 | 10.00±0.33 | 25 |
| | $N_{30}$ | 13.96±0.59 | 37.38±0.02 | 10.46±0.45 | 8 |
| | $S_{Full}$ | 13.49±1.27 | 37.74±0.05 | 6.03±0.34 | 17 |
| S5 | $S_3$ | 42.45±2.60 | 37.28±0.03 | 7.44±0.33 | 6 |
| | $S_6$ | 60.63±4.96 | 36.66±0.04 | 7.94±0.50 | 1 |
| | $H_{Full}$ | 6.63±0.42 | 37.98±0.03 | 9.97±0.62 | 31 |
| H1013 | $H_4$ | 11.15±0.52 | 37.52±0.02 | 10.33±0.49 | 11 |
| | $H_6$ | 14.34±0.87 | 36.65±0.03 | 11.38 ±0.78 | 1 |

[a]Normalized to $H\beta$=100.

# Conclusions (M33)

- IFS covering from 3600Å to 1μm (from [OII] to [SIII]) for 2 starforming regions in M33 was obtained with PPAK in Calar Alto. A central area 300×500 $pc^2$ and IC132 at 19´ (4.69 kpc) galactocentric distance.
J. López et al. 2013, MNRAS, 430, 472

- Physical conditions for each spaxel and integrated over iso-Hα surface brightness were derived.

- Many spaxels in the [SII] ratio maps ($N_e$) were found outside the theoretical limits.

Oosterbrock

Electron density can also be determined from
ratios of certain emission lines. e.g. [OII] y [SII]

DENSITY

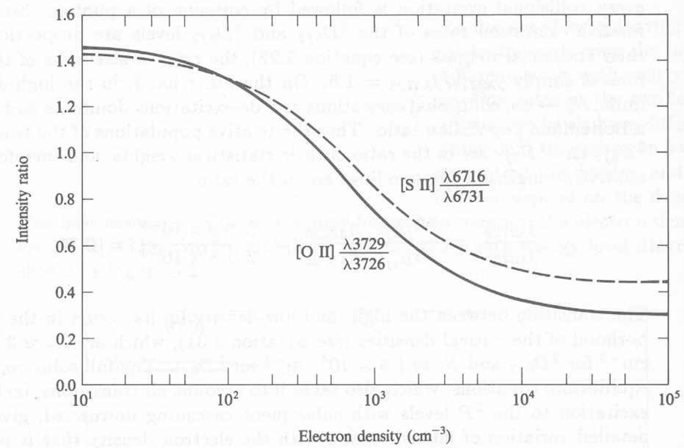


FIGURE 5.3
Calculated variation of [O II] (*solid line*) and [S II] (*dashed line*) intensity ratios as function of $N_e$ at $T = 10,000°$ K. At other temperatures the plotted curves are very nearly correct if the horizontal scale is taken to be $N_e(10^4/T)^{1/2}$.

# Conclusions (M33)

- IFS covering from 3600Å to 1μm (from [OII] to [SIII]) for 2 starforming regions in M33 was obtained with PPAK in Calar Alto. A central area 300×500 $pc^2$ and IC132 at 19´ (4.69 kpc) galactocentric distance.
  J. López et al. 2013, MNRAS, 430, 472
- Physical conditions for each spaxel and integrated over iso-Hα surface brightness were derived.
- Many spaxels in the [SII] ratio maps ($N_e$) were found outside the theoretical limits. This calls for a revision in the collisional strengths for the theoreticians.
  (Watch this space; Ferland, private communication).

- Higher temperatures, EW(Hβ), size and excitation are observed and lower direct and empirical abundances and extinction are derived in the outer relative to the inner regions.
- Evidence for diffuse emission is found in the external region.
- With this pilot programme we proved the feasibility of the project.

- BPT diagnostic diagrammes reveal two different sequences for the central and outer regions. Photoionization models explain them mainly as due to ionization parameter (U) and to a lesser degree, to Z. They also show that one cannot use global diagnostic diagrammes when analysing "fractional" 3D data.
- Two concentrations of Wolf-Rayet features are detected in IC132. Their integrated spectra are consistent with them hosting 21 and 24 WN7 stars respectively.
- No WR stars were found in the central regions in spite of their higher metallicities. (???)

# (M101)

- 3 HII regions were observed with IFS in M101 using GMOS at Gemini-N.
- The difference in scale between the two telescopes is compensated by the difference in distance of the two galaxies, so the spatial resolution of both sets of observations is comparable.
- No inconsistencies were found in these regions with the determinations of electron densities from [SII] ratios (could different abundances explain that?  8.9 - 8.5 for M33 vs. 8.74 - 7.55 for M101)

- The results are mostly consistent with homogeneous properties inside each HII region.
- WR features were found in the three regions, both WN and WC stars, helping to pin down the age of the ionizing clusters. Aperture effects were studied, higher spatial resolution is highly desirable.
- The spaxels again populate different regions in the BPT diagrams. Full 3D photoionization models are in progress
  (with C. Morisset, watch this space, too)

Sta. María Tonantzintla

# Welcome to Mexico!